Research Article | Vol. 26, No. 8 | 16 Apr 2018 | OPTICS EXPRESS 10382
Optics EXPRESS

High resolution channeled imaging spectropolarimetry based on liquid crystal variable retarder

TINGYU YAN,[1] CHUNMIN ZHANG,[1,4] JIRUI ZHANG,[1] NAICHENG QUAN,[2] AND CUNCUN TONG[3,5]

[1]*Institute of Space Optics, School of Science, Xi'an Jiaotong University, Xi'an Shaanxi 710049, China*
[2]*School of Materials Science and Engineering, Xi'an University of Technology, Xi'an Shaanxi 710048, China*
[3]*Affiliated Hospital of Shaanxi University of Chinese Medicine, Xianyang Shaanxi 712000, China*
[4]*zcm@xjtu.edu.cn*
[5]*tcc8632@163.com*

Abstract: A method for high spectral resolution channeled imaging spectropolarimetry (CISP) using a liquid crystal variable retarder (LCVR) is presented. Controlling the retardation of LCVR, the individual expanded channel, which takes up the whole detector, is obtained in each step. The resolution of recovered spectrum is increased largely, meanwhile the high resolution of image is maintained. The novel CISP system has the advantages of high throughput, compact and stable. It has no moving components and is easy to control as the retardation of LCVR is modulated by computer. The feasibility of that method is proved by the simulation results.

© 2018 Optical Society of America under the terms of the OSA Open Access Publishing Agreement

OCIS codes: (110.4234) Multispectral and hyperspectral imaging; (120.6200) Spectrometers and spectroscopic instrumentation; (260.5430) Polarization; (300.6300) Spectroscopy, Fourier transforms.

References and links

1. C. Zhang, Q. Li, T. Yan, T. Mu, and Y. Wei, "High throughput static channeled interference imaging spectropolarimeter based on a Savart polariscope," Opt. Express **24**(20), 23314–23332 (2016).
2. J. S. Tyo, D. L. Goldstein, D. B. Chenault, and J. A. Shaw, "Review of passive imaging polarimetry for remote sensing applications," Appl. Opt. **45**(22), 5453–5469 (2006).
3. T. G. Moran and J. M. Davila, "Three-dimensional polarimetric imaging of coronal mass ejections," Science **305**(5680), 66–70 (2004).
4. R. S. Gurjar, V. Backman, L. T. Perelman, I. Georgakoudi, K. Badizadegan, I. Itzkan, R. R. Dasari, and M. S. Feld, "Imaging human epithelial properties with polarized light-scattering spectroscopy," Nat. Med. **7**(11), 1245–1248 (2001).
5. K. Oka and T. Kato, "Spectroscopic polarimetry with a channeled spectrum," Opt. Lett. **24**(21), 1475–1477 (1999).
6. S. Jones, F. Iannarilli, and P. Kebabian, "Realization of quantitative-grade fieldable snapshot imaging spectropolarimeter," Opt. Express **12**(26), 6559–6573 (2004).
7. J. S. Tyo and T. S. Turner, Jr., "Variable-retardance, Fourier-transform imaging spectropolarimeters for visible spectrum remote sensing," Appl. Opt. **40**(9), 1450–1458 (2001).
8. R. W. Aumiller, C. Vandervlugt, E. L. Dereniak, R. Sampson, and R. W. McMillan, "Snapshot imaging spectropolarimetry in the visible and infrared," Proc. SPIE **6972**, 69720D (2008).
9. J. M. Craven and M. W. Kudenov, "False signature reduction in channeled spectropolarimetry," Opt. Eng. **49**(5), 053602 (2010).
10. D. H. Goldstein, *Polarized Light,* 3rd ed. (CRC Press, 2010).
11. C. Zhang, B. Xiangli, B. Zhao, and X. Yuan, "A static polarization imaging spectrometer based on a Savart polariscope," Opt. Commun. **203**(1–2), 21–26 (2002).
12. T. Yan, C. Zhang, Q. Li, Y. Wei, and J. Zhang, "Efficient background removal based on two-dimensional notch filtering for polarization interference imaging spectrometers," Chin. Opt. Lett. **14**(12), 123002 (2016).
13. C. Zhang, X. Yan, and B. Zhao, "A novel model for obtaining interferogram and spectrum based on the temporarily and spatially mixed modulated polarization interference imaging spectrometer," Opt. Commun. **281**(8), 2050–2056 (2008).
14. X. Jian, C. Zhang, L. Zhang, and B. Zhao, "The data processing of the temporarily and spatially mixed modulated polarization interference imaging spectrometer," Opt. Express **18**(6), 5674–5680 (2010).

#322590 https://doi.org/10.1364/OE.26.010382
Journal © 2018 Received 6 Feb 2018; revised 2 Apr 2018; accepted 2 Apr 2018; published 10 Apr 2018

Optics EXPRESS

1. Introduction

Useful information can be obtained from the image, spectrum and polarization of the object. Imaging spectropolarimetry is capable of capturing image and spectrum of four Stokes parameters simultaneously [1]. It has been considered as a powerful tool to acquire the characteristics of object in many fields, such as environmental monitoring, object identification, and biomedical diagnoses [2–4]. One of the most representative technique is channeled imaging spectropolarimetry (CISP) [1]. Channeled spectropolarimetry (CSP) was developed by Oka and Kato [5]. Using a pair of high order crystal retarders as polarization spectrum modulation components, it can detect the total Stokes parameters simultaneously without movable components by modulating the Stokes parameters S_1, S_2 and S_3 into a finely-vibrating spectrum. Behind the polarization spectral modulation components, some typical imaging spectrometers such as grating imaging spectrometer (GIS) [6], Fourier transform imaging spectrometer (FTIS) [7] and computed tomography imaging spectrometer (CTIS) [8] are implemented to analyze the complicated modulated spectrum and get the image. Zhang et al presented a high throughput static channeled interference imaging spectropolarimeter based on Savart polariscope, which offers a robust system and a high optical throughput to resist the instrument noise [1].

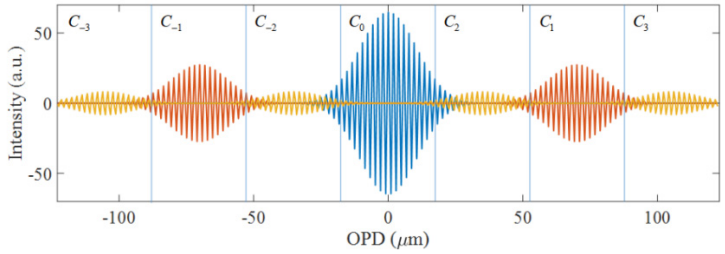

Fig. 1. Seven-channel interferogram. The aliasing between channels can be seen obviously because of the short OPD for each channel.

However, the resolution of recovered spectrum is severely limited by the much shorter length of channels and aliasing between channels, which is also a defect of CSP [9]. As is shown in Fig. 1, on the CCD detector plane we can get a seven-channel interferogram. It is obviously that each channel takes up only one seventh of the CCD plane, as a result, the optical path difference (OPD) of each channel is only one seventh of interferogram captured by traditional FTISs. According to the relationship between spectral resolution and OPD, after windowing and intercepting, the resolution of recovered spectrum drops down greatly compared with FTISs. Craven et al described a theoretical means for improving the spectral resolution of CSP by at least a factor of four [9]. But the crystal retarders must be rotated twice and it is difficult to operate in practice. How to obtain large OPD interferogram without sacrificing the compact and static advantages of CSP is always the difficulty in this research field, few achievements is reported. In this paper, we present a novel CISP (NCISP) based on liquid crystal variable retarders (LCVR), which takes advantages of liquid crystal modulation and CISP based on Savart polariscope.

Optics EXPRESS

2. Theoretical analysis

2.1 Optical layout and principle

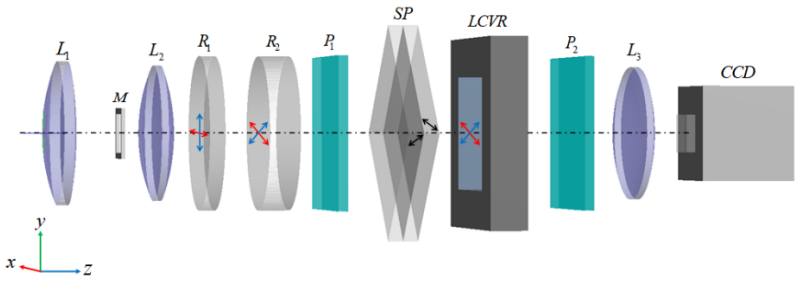

Fig. 2. Optical layout of the NCISP based on a LCVR. The red axis represents fast axis of the crystal retarders and LCVR.

The layout of the system is shown in Fig. 2, the first part is fore-optics, in which a field stop instead of a slit is implemented to ensure high optical throughput. After that the collimating light beam incident into polarization spectral modulation components. Fast axes of two birefringent crystal retarders, R_1 and R_2, orientations at 0° and 45° relative to the horizontal. The analyzer behind R_2 in CSP can be combined with the linear polarizer P_1 in the imaging spectrometer based on Savart polariscope. The transmission axes of P_1 and analyzer P_2 are orientation at horizontal, aligned with the fast axes of R_1. The Savart polariscope SP is rotated clockwise along z axis by 45° The optic axes of the two plates are oriented at 45° relative to z axis and their projections on x-y plane are oriented at $\pm 45^\circ$ respectively relative to x axis [1]. In the NCISP, a LCVR is implemented. It can offer variable phase-only retardance, which has the characteristic of time modulation. The orientation of fast axes of liquid crystal is same as R_2. Finally, using a reimaging lens L_3, the image of the object overlapped with channeled interferogram is focused on the CCD, which is placed on the back focal plane of L_3.

According to the principle of polarization optics, the polarization state of the light from the target can be described by Stokes vector. It is defined as [10]

$$\mathbf{S}(\sigma)=\begin{bmatrix} S_0(\sigma) \\ S_1(\sigma) \\ S_2(\sigma) \\ S_3(\sigma) \end{bmatrix}=\begin{bmatrix} I_{0^\circ}(\sigma)+I_{90^\circ}(\sigma) \\ I_{0^\circ}(\sigma)-I_{90^\circ}(\sigma) \\ I_{45^\circ}(\sigma)-I_{135^\circ}(\sigma) \\ I_R(\sigma)-I_L(\sigma) \end{bmatrix} \tag{1}$$

where $S_0(\sigma)$ is the total intensity of the light, $S_1(\sigma)$ is the difference between the intensity of the linearly polarized light in 0° direction and 90° direction, $S_2(\sigma)$ is the difference between the intensity of the linearly polarized light in 45° direction and 135° direction, and $S_3(\sigma)$ is the difference between the intensity of the right circularly polarized light and the left circularly polarized light.

The polarization characteristics of any optical element can be represented by a Mueller matrix, which is a 4×4 matrix. The relationship between the polarization state of the incident light and the emergent light from optical element can be described as [10]

Optics EXPRESS

$$\mathbf{S}_{\text{out}} = \begin{bmatrix} S_{0\_out} \\ S_{1\_out} \\ S_{2\_out} \\ S_{3\_out} \end{bmatrix} = \begin{bmatrix} m_{00} & m_{01} & m_{02} & m_{03} \\ m_{10} & m_{11} & m_{12} & m_{13} \\ m_{20} & m_{21} & m_{22} & m_{23} \\ m_{30} & m_{31} & m_{32} & m_{33} \end{bmatrix} \begin{bmatrix} S_{0\_in} \\ S_{1\_in} \\ S_{2\_in} \\ S_{3\_in} \end{bmatrix} = \mathbf{M}\mathbf{S}_{\text{in}} \tag{2}$$

where $\mathbf{M}$ is the Mueller matrix of the optical element, and Eq. (2) is called Mueller calculus. It is noted that each Stokes parameter is a function of wavenumber σ, which is omitted in the equation.

The principle of NCISP can be descried by Mueller calculus. Using the Mueller matrices of those components, the Stokes vector of the emergent light from P_2 can be described as

$$\mathbf{S}_{\text{out}} = \mathbf{M}_{\mathbf{P}_2}\mathbf{M}_{\text{LCVR}}\mathbf{M}_{\text{SP}}\mathbf{M}_{\mathbf{P}_1}\mathbf{M}_{\mathbf{R}_2}\mathbf{M}_{\mathbf{R}_1}\mathbf{S}_{\text{in}} \tag{3}$$

where $\mathbf{M}_{\mathbf{P}_2}$, $\mathbf{M}_{\text{LCVR}}$, $\mathbf{M}_{\text{SP}}$, $\mathbf{M}_{\mathbf{P}_1}$, $\mathbf{M}_{\mathbf{R}_2}$ and $\mathbf{M}_{\mathbf{R}_1}$ are the Mueller matrices of the analyzer P_2, the LCVR, the SP, the polarizer P_1, the retarders R_2 and R_1, respectively. In our system, the SP can be regarded as a combine of two retarders, and the LCVR work as a pure phase retarder. As a result, we can model them using the Mueller matrix of a retarder. According to the retardance and the orientation of the optic axes of SP and LCVR, the Mueller matrices of them can be written as [10,11]

$$\mathbf{M}_{\text{SP}} = \begin{bmatrix} 1 & 0 & 0 & 0 \\ 0 & \cos\varphi_{SP} & 0 & -\sin\varphi_{SP} \\ 0 & 0 & 1 & 0 \\ 0 & \sin\varphi_{SP} & 0 & \cos\varphi_{SP} \end{bmatrix} \tag{4}$$

$$\mathbf{M}_{\text{LCVR}} = \begin{bmatrix} 1 & 0 & 0 & 0 \\ 0 & \cos\varphi_{LCVR} & 0 & -\sin\varphi_{LCVR} \\ 0 & 0 & 1 & 0 \\ 0 & \sin\varphi_{LCVR} & 0 & \cos\varphi_{LCVR} \end{bmatrix} \tag{5}$$

Since CCD detector do not respond to polarization states, only S_{0_out} can be measured. As a result, the radiation intensity distributed on CCD plane can be expressed as

$$\begin{aligned} I_{CCD} &= S_{0\_out} \\ &= \frac{1}{4}(1 + \cos\varphi_{LCVR}\cos\varphi_{SP} - \sin\varphi_{LCVR}\sin\varphi_{SP})S_0' \end{aligned} \tag{6}$$

where

$$\begin{aligned} S_0' &= S_{0\_in} + S_{1\_in}\cos\varphi_2 \\ &\quad + S_{2\_in}\sin\varphi_1\sin\varphi_2 - S_{3\_\text{in}}\cos\varphi_1\sin\varphi_2 \end{aligned} \tag{7}$$

And the phase terms in above equations are given by

$$\varphi_{LCVR}(\sigma) = 2\pi B_{LCVR}(\sigma)d_{LCVR}\sigma \tag{8}$$

$$\varphi_{SP}(\sigma) = 2\pi\Delta_{SP}\sigma \tag{9}$$

$$\varphi_1(\sigma) = 2\pi B(\sigma)d_1\sigma \tag{10}$$

$$\varphi_2(\sigma) = 2\pi B(\sigma)d_2\sigma \tag{11}$$

Optics EXPRESS

where $B_{LCVR}(\sigma)$, $B(\sigma)$, d_{LCVR}, and d_i, $(i=1,2)$ are the birefringence and thicknesses of the liquid crystal and two retarders, respectively. Δ_{SP} is the OPD from SP. The thicknesses of R_1 and R_2 are chosen to be $d_1 = d_2/2$ to make each channel length equal in the interferogram. By expanding Eq. (6) and Eq. (7), a channel-form expression of I_{CCD} can be described as

$$\begin{aligned} I_{CCD} &= \frac{[1+\cos(\varphi_{SP}+\varphi_{LCVR})]}{4}[S_0 + \frac{S_1}{2}e^{i\varphi_2} + \frac{S_1}{2}e^{-i\varphi_2} \\ &+ \frac{S_2+iS_3}{4}e^{-i(\varphi_1-\varphi_2)} + \frac{S_2-iS_3}{4}e^{i(\varphi_1-\varphi_2)} \\ &+ \frac{-S_2+iS_3}{4}e^{i(\varphi_1+\varphi_2)} + \frac{-S_2-iS_3}{4}e^{-i(\varphi_1+\varphi_2)}] \\ &= \frac{[1+\cos(\varphi_{SP}+\varphi_{LCVR})]}{4}[C_0 + C_{-1} + C_1 + C_{-2} + C_2 + C_{-3} + C_3] \end{aligned} \tag{12}$$

It is obviously that the Stokes parameters S_1, S_2 and S_3 are modulated into special channels, respectively. In practice, incident light is a broadband spectrum, and the radiation intensity is an integration for wavenumber σ. As a result, I_{CCD} becomes a function of OPD. It is the interferogram and changes along with the angle of field of view (FOV). And the position of each channel is centered at specific OPD. From Eq. (12), φ_{SP} and φ_{LCVR} both contribute to OPD, which is the principle of channel moving. By controlling the birefringence of the LCVR, φ_{LCVR} is changed, and the zero OPD position is moved, along with the channels. In NCISP, we can reconstruct the polarization spectrum using only three channels C_0, C_1 and C_2, and those channels are supposed to take up the whole CCD plane, respectively. To achieve that goal, we need to expand the channel length. Suppose that $\Delta_{\max}$ is the maximum OPD provided by SP, and according to the relationship between OPD and center positions of C_1 and C_2, we have

$$\Delta_{R_2} = 4\Delta_{\max} \tag{13}$$

$$\Delta_{R_2} - \Delta_{R_1} = 2\Delta_{\max} \tag{14}$$

where Δ_{R_2} and $\Delta_{R_2} - \Delta_{R_1}$ are the center positions of C_1 and C_2, respectively. Δ_{R_1} and Δ_{R_2} are the products of birefringence and thicknesses of R_1 and R_2, means the OPD provided by R_1 and R_2. That is to say, the center positions of C_1 and C_2 are $4\Delta_{\max}$ and $2\Delta_{\max}$ from the center of CCD plane, respectively. According to Eq. (12), the phase differences between the center position of C_1 and the center of CCD plane are $2\pi\Delta_{R_2}\sigma$, which is $2\pi(\Delta_{R_2}-\Delta_{R_1})\sigma$ for C_2. After that, we need to move C_0, C_1, and C_2 to the center of CCD plane using three specific retardances of LCVR, which are 0, $8\pi\Delta_{\max}\sigma$ and $4\pi\Delta_{\max}\sigma$. As a pure phase retarder, the retardances of LCVR can be controlled by computer, so it is better to set the order of retardances as 0, $4\pi\Delta_{\max}\sigma$ and $8\pi\Delta_{\max}\sigma$ to get a continuous modulation. As a result, the process contains three steps. Ignoring the aliasing effect of other channels, the radiation intensity distributed on CCD plane in each step can be expressed as

$$I_{step1}(\Delta) = \int \frac{[1+\cos(\varphi_{SP})]}{4} S_0 d\sigma \tag{15}$$

$$I_{step2}(\Delta) = \int \frac{[1+\cos(\varphi_{SP})]}{4} (\frac{S_2 - iS_3}{4}) d\sigma \tag{16}$$

Optics EXPRESS

$$I_{step3}(\Delta)=\int\frac{[1+\cos(\varphi_{SP})]}{4}(\frac{S_1}{2})d\sigma \tag{17}$$

Unlike the windowing and intercepting procedure in typical CISP, the three channels are isolated by CCD plane directly, without subsequent process by computer. What' s more, the center of each channel is exactly on the center of CCD plane in each step, which means phase correction is unnecessary in NCISP. Therefore, spectral recovery process is greatly simplified. After background removal [12], using fast Fourier transform (FFT), the spectrally-dependent Stokes parameters can be demodulated as follows

$$S_0(\sigma)=4\Im\{I_{step1}(\Delta)\} \tag{18}$$

$$S_1(\sigma)=8\Im\{I_{step3}(\Delta)\} \tag{19}$$

$$S_2(\sigma)=16\text{real}(\Im\{I_{step2}(\Delta)\}) \tag{20}$$

$$S_3(\sigma)=-16\text{imag}(\Im\{I_{step2}(\Delta)\}) \tag{21}$$

Each Stokes parameter has a specific shape of spectrum, which means that the Stokes characteristics will be understandable after normalization. In fact, $S_1(\sigma)/S_0(\sigma)$, $S_2(\sigma)/S_0(\sigma)$, and $S_3(\sigma)/S_0(\sigma)$ are the normalized Stokes parameters while $S_0(\sigma)$ is the natural spectrum of objects.

2.2 Detection mode

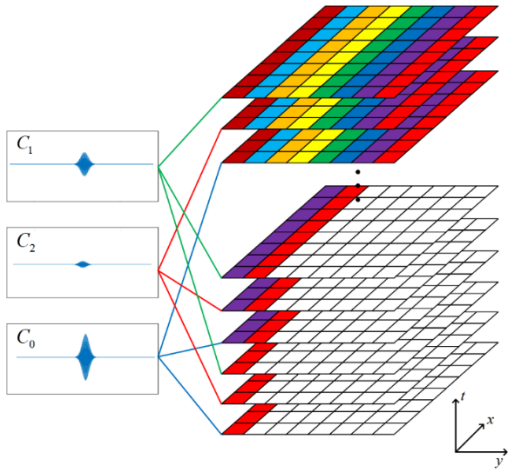

Fig. 3. Data acquisition model of the NCISP system.

The detection mode of NCISP is the combine of windowing mode [13,14] and temporal modulation mode. The data acquisition model is shown in Fig. 3. The FOV of NCISP system moves over the whole detection area using translation stage or turntable. However, it is not a continuous scanning but a step scanning process. In each scanning position, three exposures are needed to get the interference intensities of every object point at its special OPD in different channels. After a whole scan, a series of images of detection area are acquired. By rearranging those images, the interferogram of each point is obtained. To get the channeled interferogram, the retardance of LCVR needs to change once in a single exposure interval, as the three steps described above. Because of the high optical throughput of the system, a shorter exposure time in each modulation step is acceptable. As is shown in Fig. 3, those images represented the same channel are arranged into one group when processing the acquired data. Hence three interferogram cubes can be obtained, in which the *xy* directions

Optics EXPRESS

represent the two-dimension image while the *t* direction is the interferogram of each object point. Figure 3 shows a simplified detection process in which the channeled interferogram of red column is completely obtained. Using the reconstruction algorithm described in *2.1*, the image, spectrum and polarization of the object can be obtained.

3. The simulation experiment of NCISP system

To prove the feasibility of NCISP, a simulation system was implemented. The NCISP system uses a CCD camera with 512 × 512 element, and has a spectrum detection range of 480nm~960nm. According to the Nyquist sampling theorem, the interferogram sampling intervals requires $\Delta\delta \le 0.48\mu m$. As a result, the maximum OPD of the NCISP system is about 123μm, and the spectral resolution of NCISP is 40cm^{-1} theoretically, which is usually several hundred cm^{-1} for traditional CISP. Then, a narrow-band polarization spectrum and a wide-band polarization spectrum with characteristic peaks were simulated to demonstrate the correctness of the principle of NCISP.

As is shown in Fig. 4, we constructed a narrow-band Gaussian line shape incident polarization spectrum, in which S_0, S_1, S_2 and S_3 are the four Stokes parameters. It is known that the conventional CISP system can only detect broad-band polarization spectrum. For the narrow-band spectrum, the channeled interferogram always has a better modulation, which means the intensity of the channeled interferogram decrease slower with the increase of OPD. As a result, the length of channels become longer, and aliasing between channels is more severe. Windowing and intercepting cannot separate those mixing channels completely, so the recovered polarization spectrums from those channels are incorrect.

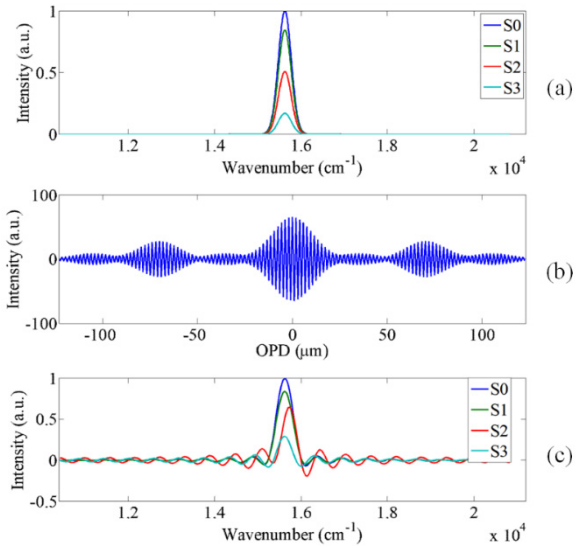

Fig. 4. (a) Narrow-band Gaussian line shape incident polarization spectrum in simulation, (b) aliasing channeled interferogram captured by conventional CISP, (c) recovered polarization spectrum captured by conventional CISP.

Optics EXPRESS

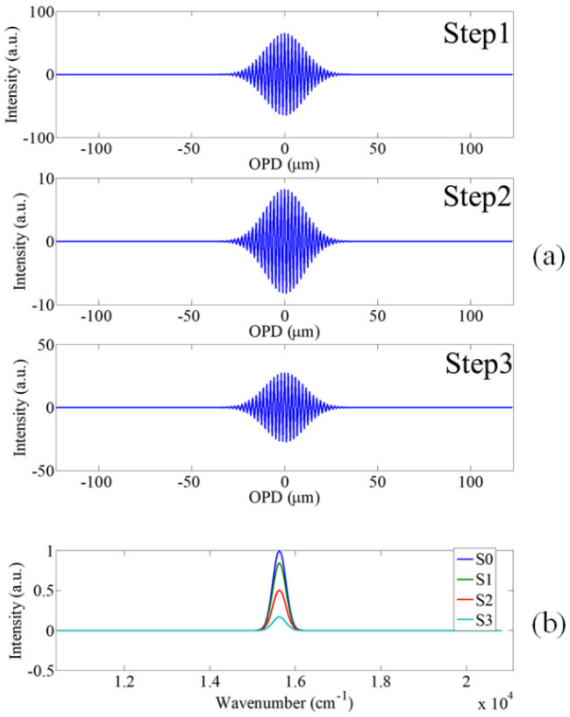

Fig. 5. (a) The three channeled interferograms of Narrow-band polarization spectrum captured in three steps, (b) recovered polarization spectrum captured using NCISP.

In our simulation experiment, the narrow-band spectrum has an average full width at half maximum of 300 cm^{-1}. The channeled interferogram acquired by conventional CISP system is shown in Fig. 4(b), in which the channels are mixed with each other, and the boundaries between neighbor channels are not clear. In a programed recovery procedure, that mixed information will affect the correctness of recovered polarization spectrum, which is shown in Fig. 4(c). We find that each recovered polarization spectrum has an obvious vibration caused by false mixed information.

When using NCISP system, the situation is much better. The three useful channeled interferograms are captured in three steps, each has a large OPD. As is shown in Fig. 5(a), the aliasing is eliminated, and the OPD is 7 times of conventional CISP. It indicates that the resolution of recovered spectrum is much higher. Figure 5(b) shows the results of recovered polarization spectrum obtained by NCISP. It is obvious that the recovered polarization spectrum using NCISP is almost the same with the incident one, which proves the feasibility of the NCISP. Besides, for the broad-band spectrum with several characteristic peaks, the advantage of NCISP is also proved in our simulations. Four Stokes spectrums are constructed and inputted into the simulation system, which is shown in Fig. 6, the aliasing between channels seems not so obvious as narrow-band spectral interferogram because of the lower modulation of wide-band spectral interferogram. However, Fig. 6(c) indicates that the aliasing still has significant effects to the recovered spectrum using conventional CISP. The condition is different when NCISP is implemented. As is shown in Fig. 7, the three selected channels have no aliasing with each other, meanwhile the OPD of each channel is expanded, and the recovered result is coincident with the incident spectrum.

Optics EXPRESS

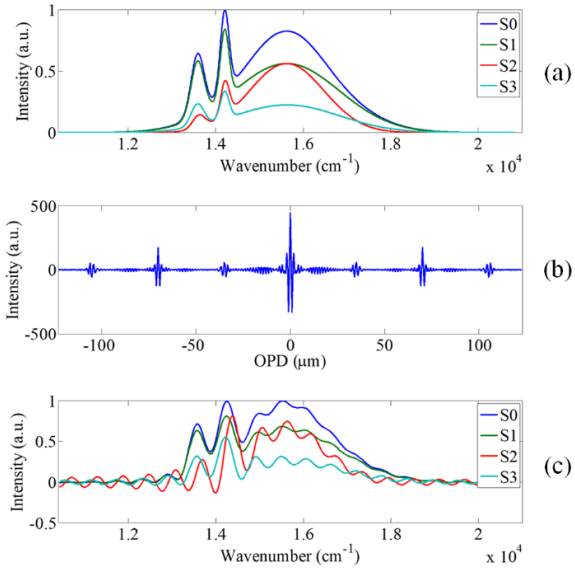

Fig. 6. (a) wide-band incident polarization spectrum with characteristic peaks in simulation, (b) aliasing channeled interferogram captured by conventional CISP, (c) recovered polarization spectrum captured by conventional CISP.

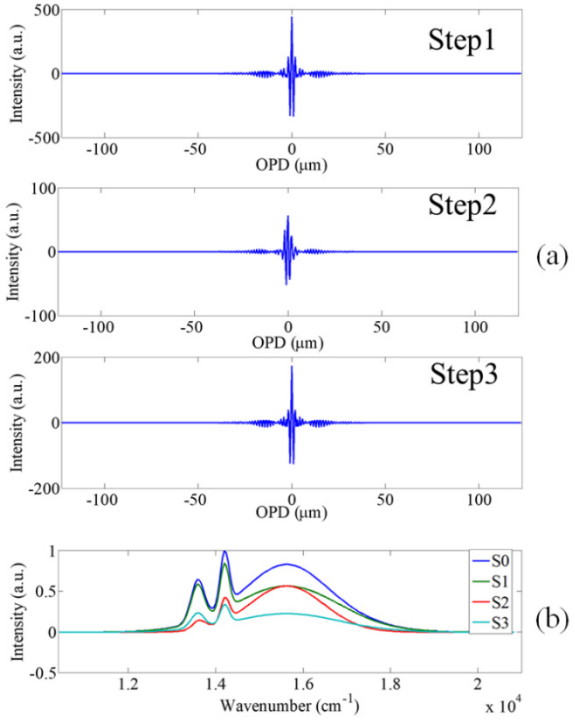

Fig. 7. (a) The three channeled interferograms of wide-band polarization spectrum with characteristic peaks captured in three steps, (b) recovered polarization spectrum captured using NCISP.

All the components are assumed to be ideal in this simulation experiment. However, there are some error sources which can influence the system performance in practice. The optical axes orientation error and the thickness error of retarders are two common error sources,

Optics EXPRESS

which can be minimized during system installation. But the residual errors still have an impact on the correctness of interferogram, and change the distance between different channels. Those errors should be eliminated by calibration, while the implementation of LCVR can reduce the influence of unequal channel spacing because it can adjust the positions of channels.

In practice, the performance of LCVR can be affected by several factors, such as dispersion, temperature, and alignment. In NCISP system, the main function of LCVR is offer a controllable retardance, which is adjustable in measurement using feedback control. In other words, the retardance of LCVR can be adapted to the operating temperature and the alignment. Besides, a temperature control system is also helpful. But the dispersion will bring serious errors when the incident light is a broadband spectrum. To compensate the dispersion of LCVR, we can insert a different birefringent crystal with a dispersion curve of opposite trend before the LCVR. What is more, we can also calculate a series correction factors for the recovered spectrum calibration using the relationship between the birefringence of LCVR and wavenumber.

4. Conclusion

In conclusion, we proposed a method for high spectral resolution CISP based on LCVR. The principle and the detection mode of NCISP system are demonstrated, and a simulation experiment is carried out. The results show that NCISP is a feasible and efficient tool to get the image, spectrum and polarization information of object simultaneously. Compared with the conventional CISP, it partly solves the aliasing problem, and expands the OPD of useful channels in a great degree. As a result, the resolution of recovered spectrum is increased largely, meanwhile the high resolution of image is maintained. The NCISP system have the advantages of high throughput, compact and stable because it has no moving components and based on Savart polariscope. The system is easy to control as the retardance of LCVR can be modulated by voltage, which is operated on computer. Automation is also possible for NCISP. Further research will focus on optimizing the characteristics of LCVR, such as its flatness, stability and transmittance.

Funding

National Natural Science Foundation of China (41530422, 61775176); Ministry of Science and Technology of the People's Republic of China (2012AA121101, 32-Y30B08-9001-13/15).

115.154.227.101 {ts '2019-06-26 23:32:42'}